INSTITUTE OF PHYSICS PUBLISHING PLASMA PHYSICS AND CONTROLLED FUSION

Plasma Phys. Control. Fusion **45** (2003) 1829–1843 PII: S0741-3335(03)64879-7

Effective ripple in the CHS-qa configuration

V V Nemov[1], M Isobe[2], W Kernbichler[3], S V Kasilov[1], K Matsuoka[2], S Okamura[2] and A Shimizu[2]

[1] Institute of Plasma Physics, National Science Center 'Kharkov Institute of Physics and Technology', Akademicheskaya str. 1, 61108 Kharkov, Ukraine
[2] National Institute for Fusion Science, Oroshi-Cho 322-6, Toki-city, Gifu-Pref. 509-5292, Japan
[3] Institut für Theoretische Physik, Technische Universität Graz, Petersgasse 16, A–8010 Graz, Austria

Received 18 June 2003
Published 15 September 2003
Online at stacks.iop.org/PPCF/45/1829

Abstract

The effective ripple is analysed for the final version of the quasi-axisymmetric stellarator configuration with a low aspect ratio, CHS-qa. For the computation, a method is used that is based on the integration along magnetic field lines in a given magnetic field. Computations are done for magnetic fields presented in Boozer magnetic coordinates as well as for magnetic fields produced directly by currents in the modular coils of the device. The computations show the significant advantage of CHS-qa over a conventional stellarator resulting from the reduced effective ripple.

1. Introduction

Among stellarator optimization studies, which are presently performed worldwide, the CHS-qa [1–3] design study occupies one of the important places. The CHS-qa is a quasi-axisymmetric stellarator configuration with a low aspect ratio, which has been considered as one of the candidates of a post-CHS [4, 5] device. A number of studies [6–9] related to different versions of the CHS-qa configuration have shown transport improvement and the possibility of its control in experiments. As a result of studies of various versions of the CHS-qa configuration, the final version 2*b*32 is chosen as the present candidate for the CHS-qa device.

The transport improvement in the so-called $1/\nu$ regime is one of the important requirements for optimized stellarator systems [10]. This improvement correlates with a decreasing effective ripple, ϵ_{eff}, obtained from neoclassical transport computations in this regime. In this paper, the effective ripple for the 2*b*32 configuration is analysed using a method based on integration along magnetic field lines in a given magnetic field [11]. Computations are performed for magnetic fields presented in Boozer magnetic coordinates [12] as well as for real-space magnetic fields directly produced by currents in the modular coils of the device.

For the magnetic field presented in Boozer coordinates, a zero beta case as well as finite beta cases are considered. For the finite beta case, a possible influence of the bootstrap current

is taken into account. This is done for $\langle\beta\rangle \approx 3\%$ with a fixed boundary equilibrium and for $\langle\beta\rangle \approx 1.5\%$ with a free boundary equilibrium. For magnetic fields directly produced by modular coils, a possible influence of an additional vertical magnetic field is also analysed. Being closely connected to the effective ripple, the bounce averaged trapped particle drift velocity across magnetic surfaces is also discussed.

From the results obtained it follows that the effective ripple for CHS-qa is essentially reduced compared to CHS. For the vacuum magnetic field this ripple is smaller than that for the finite beta equilibrium that takes bootstrap current into account. However, even in this less favourable case the effective ripple for CHS-qa is significantly smaller than those for conventional stellarator configurations.

2. Effective ripple and $1/\nu$ neoclassical transport

Minimization of the effective ripple, $\epsilon_{\rm eff}$, obtained from neoclassical transport computations in the $1/\nu$ regime is one of the key issues in stellarator optimization (see, e.g. [10]). In the $1/\nu$ regime, the $\epsilon_{\rm eff}$ value enters the expression for transport coefficients as a factor $\epsilon_{\rm eff}^{3/2}$. For a conventional stellarator field, $\epsilon_{\rm eff}$ coincides with the helical ripple $\epsilon_{\rm h}$ (see, e.g. [13]). For an arbitrary stellarator magnetic field, in accordance with [11], the quantity $\epsilon_{\rm eff}^{3/2}$ can be calculated with the help of the following expression:

$$\epsilon_{\rm eff}^{3/2} = \frac{\pi R_0^2}{8\sqrt{2}} \lim_{L_s\to\infty} \left(\int_0^{L_s} \frac{{\rm d}s}{B}\right) \left(\int_0^{L_s} \frac{{\rm d}s}{B} |\nabla\psi|\right)^{-2} \int_{B_{\rm min}^{\rm abs}/B_0}^{B_{\rm max}^{\rm abs}/B_0} {\rm d}b' \sum_{j=1}^{j_{\rm max}} \frac{\hat{H}_j^2}{\hat{I}_j},$$
$$\hat{H}_j = \frac{1}{b'} \int_{s_j^{\rm min}}^{s_j^{\rm max}} \frac{{\rm d}s}{B} \sqrt{b' - \frac{B}{B_0}} \left(4\frac{B_0}{B} - \frac{1}{b'}\right) |\nabla\psi| k_G, \qquad \hat{I}_j = \int_{s_j^{\rm min}}^{s_j^{\rm max}} \frac{{\rm d}s}{B} \sqrt{1 - \frac{B}{B_0 b'}}. \tag{1}$$

Here, R_0 is the major radius of the torus, B_0 is a reference magnetic field, ψ is the magnetic surfaces label, $k_G = (\boldsymbol{h} \times (\boldsymbol{h}\cdot\nabla)\boldsymbol{h}) \cdot \nabla\psi/|\nabla\psi|$ is the geodesic curvature of a magnetic field line with the unit vector $\boldsymbol{h} = \boldsymbol{B}/B$.

The quantity $\epsilon_{\rm eff}$ is calculated by integration over the magnetic field line length, s, over the sufficiently large interval 0–L_s, and by integration over the perpendicular adiabatic invariant of trapped particles, $J_\perp$, by means of the variable b'. Here, $B_{\rm min}^{\rm abs}$ and $B_{\rm max}^{\rm abs}$ are the minimum and maximum values of B within the interval 0–L_s. The quantities $s_j^{\rm min}$ and $s_j^{\rm max}$ within the sum over j in (1) correspond to the turning points of trapped particles.

For a magnetic field originally available in real-space coordinates, there is no necessity in a field transformation to magnetic coordinates. In this case, formulae (1) must be supplemented with the magnetic field line equations as well as with the equations for the vector $\boldsymbol{P} \equiv \nabla\psi$ (see, e.g. [11, 14])

$$\frac{{\rm d}P_i}{{\rm d}s} = -\frac{1}{B} \frac{\partial B^j}{\partial \xi^i} P_j, \tag{2}$$

where B^j are the contra-variant components of $\boldsymbol{B}$ in real-space coordinates ξ^i, and $P_j = \partial\psi/\partial\xi^j$ are the covariant components of $\boldsymbol{P}$.

For calculations in Boozer coordinates [12] the quantity $|\nabla\psi|k_G$ can be presented as [15]

$$|\nabla\psi| k_G = \frac{1}{B^2} (\boldsymbol{B} \times \nabla B) \cdot \nabla\psi = \frac{1}{F + \iota I} \left(I \frac{\partial B}{\partial\varphi} - F \frac{\partial B}{\partial\theta}\right) \tag{3}$$

and integration along magnetic field lines should be carried out using the field line elements

$$\frac{{\rm d}s}{B} = \sqrt{g}\, {\rm d}\varphi, \qquad \theta = \theta_0 + \iota\varphi, \qquad \sqrt{g} = \frac{1}{\nabla\psi \times \nabla\theta \cdot \nabla\varphi} = \frac{F + \iota I}{B^2} \tag{4}$$

with $\sqrt{g}$ being the metric tensor determinant. Here, θ and φ are the Boozer angle-like magnetic coordinates, $cF(\psi)/2$ and $cI(\psi)/2$ are the poloidal (external with respect to the magnetic surface) and toroidal electric currents, ι is the rotational transform in units of 2π, $\psi = \Phi/(2\pi)$ and Φ is the toroidal magnetic flux. To calculate the quantity $\nabla\psi$ one can use the relation with the normal to the magnetic surface, $\boldsymbol{N}$,

$$\nabla\psi = \frac{1}{\sqrt{g}}\boldsymbol{N}, \qquad \boldsymbol{N} = \frac{\partial \boldsymbol{r}}{\partial\theta} \times \frac{\partial \boldsymbol{r}}{\partial\varphi} \tag{5}$$

and make use of the Boozer spectra for the coordinates of a magnetic surface.

3. Magnetic field for effective ripple calculations

The $2b32$ configuration corresponds to a quasi-axisymmetric stellarator with the following main parameters: aspect ratio of $A = 3.2$; major radius $R_0 = 1.5m$; number of field periods (along the torus) $n_\mathrm{p} = 2$; and total number of modular coils is 20. Figure 1(a) shows the coil system and the outermost magnetic surface for this configuration.

Briefly, the procedure of determination of the $2b32$ magnetic field is described as follows: the sets of data that are necessary for effective ripple computations are prepared using the finite beta equilibrium code VMEC [16], which was adapted for conversion to Boozer coordinates. To find the shape of a boundary surface for an optimized configuration, this code was inserted into an optimization loop. The basic optimization goals are the reduction of the non-axisymmetric components of the Boozer spectrum of the magnetic field strength together with good properties of MHD stability, avoidance of dangerous low order resonances, etc. Optimization runs are carried out for a zero beta equilibrium with a fixed boundary.

The resulting optimized boundary is then used to determine finite beta equilibria with bootstrap current again using VMEC. The bootstrap current is calculated by the SPBSC

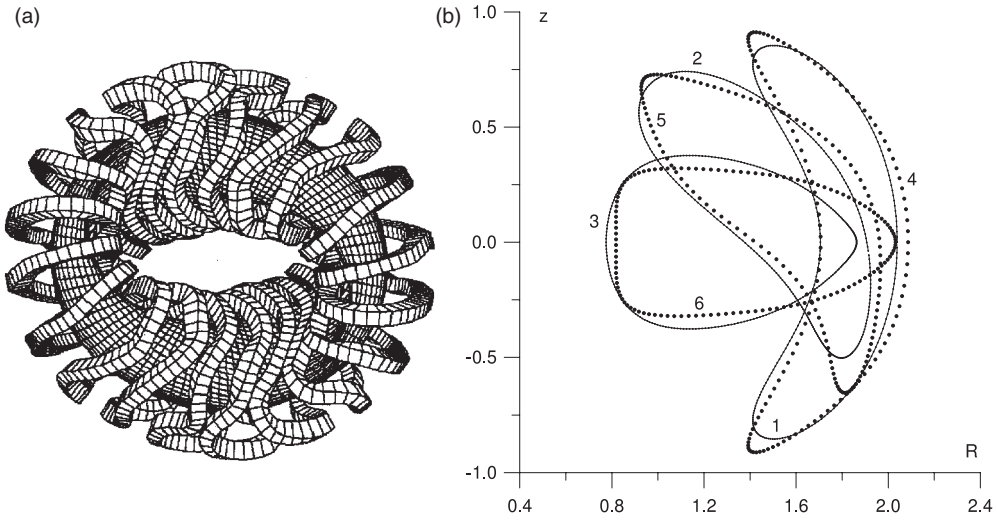

Figure 1. (a) Coil system and outermost magnetic surface for the $2b32$ configuration. (b) Cross-sections of boundary surfaces for the $2b32$ configuration for $\varphi = 0$ (curves 1 and 4), $\varphi = \pi/4$ (curves 2 and 5) and $\varphi = \pi/2$ (curves 3 and 6); solid lines represent the fixed boundary that is also the starting boundary for free boundary calculations; dots represent the final boundary for the free boundary equilibrium.

code [17] (we use pure-QA condition for bootstrap current [18]) and has been studied for CHS-qa as well as for CHS in [19]. The same optimized boundary is used as a starting boundary for the computation of a free boundary VMEC equilibrium also taking into account bootstrap current. All those VMEC equilibria are converted to Boozer coordinates. Finally, the optimized boundary is used to compute the shapes of the modular coils and the respective currents using the NESCOIL code [20, 21]. Here, it became necessary to further optimize the coil shapes and currents in order to reduce the residual mirror ripple in the magnetic field produced by the 20 modular coils. A more detailed discussion of all these topics can be found in [6, 9].

For effective ripple computations in Boozer coordinates one needs the Boozer spectrum of the magnetic field strength as well as Boozer spectra of cylindrical coordinates of the magnetic surfaces. For each equilibrium, data sets with 578 harmonics for every quantity are used. The radial dependences are determined on a set of discrete radial mesh points $s_k = (k - 0.5)/60$, $k = 1, 2, \ldots, 60$. For the magnetic field produced by modular coils, a closed filamentary conductor split into 48 short straight conductors models each of the coils. The magnetic field and its spatial derivatives are calculated on the basis of the Biot–Savart law.

4. Computational results for CHS-qa

For all computations of $\epsilon_{\rm eff}^{3/2}$ with the help of formula (1), on all flux surfaces the Boozer component B_{00} is used as the reference magnetic field B_0.

For intact magnetic surfaces, the integration is carried out over an integration interval of 250 magnetic field periods. For island magnetic surfaces as well as for their close vicinity it is necessary to increase the integration interval several times.

4.1. Effective ripple in magnetic coordinates

Results related to effective ripple computations in magnetic coordinates are presented in figures 1(*b*) and 2. Figure 1(*b*) shows cross-sections of the boundary surface used for obtaining the Boozer spectra.

In figure 2, values for $\epsilon_{\rm eff}^{3/2}$ are given as functions of r/a with r being the mean radius of a flux surface and a being the mean radius of the boundary surface.

In magnetic coordinates, the r/a value is approximated by the $\sqrt{s}$ value with s being the normalized toroidal magnetic flux inside the flux surface (the normalization flux is the flux inside the boundary surface). Curve 1 gives results for the zero beta case, which has been chosen for the boundary surface shape determination during the optimization. Curves 2 and 3 correspond to the finite beta equilibria with a fixed boundary ($\langle\beta\rangle \approx 3\%$) with finite bootstrap current and with zero toroidal current, respectively. Curve 4 relates to the free boundary equilibrium with finite bootstrap current and $\langle\beta\rangle \approx 1.5\%$. In all these cases, the criteria of local Mercier stability and of local ballooning stability are satisfied. In cases with finite bootstrap current, this current corresponds to the $1/\nu$ neoclassical transport regime.

For comparison, curve 5 in figure 2 gives results for the magnetic field produced by the modular coils (after additional optimization). This case is discussed in the next section in detail.

It is of interest to compare the obtained results with the corresponding results for different optimized configurations, particularly for the well studied optimized configuration W7-X [10]. From figure 2, it follows that for the equilibrium with a fixed boundary, in general, the level of $\epsilon_{\rm eff}^{3/2}$ does not exceed the corresponding level for W7-X ($\epsilon_{\rm eff}^{3/2} \approx 10^{-3}$) computed by the same method in [22].

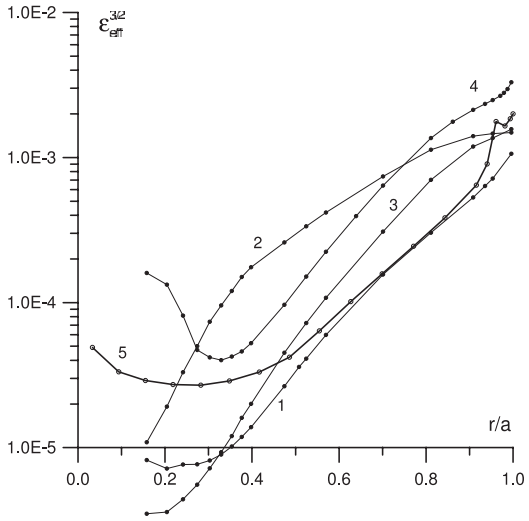

Figure 2. Parameter $\epsilon_{\rm eff}^{3/2}$ in the 2*b*32 configuration with magnetic field in Boozer coordinates for the zero beta case (curve 1); for the fixed boundary equilibrium $\langle\beta\rangle \approx 3\%$ with bootstrap current (curve 2) and with negligible bootstrap current (curve 3); for the free boundary equilibrium $\langle\beta\rangle \approx 1.5\%$ with bootstrap current (curve 4). Curve 5 shows the results for the vacuum magnetic field produced by modular coils (after additional optimization).

In a significant part of the confinement region except the near-edge part, $\epsilon_{\rm eff}^{3/2}$ is smaller for the zero toroidal current cases as for the equilibrium with bootstrap current. Results for zero toroidal current turn out to be of the same level as for the quasi-helically symmetric stellarator [23] (see results for the QHS configuration in [11]).

For the free boundary equilibrium with finite bootstrap current it turns out that for $\langle\beta\rangle \approx 3\%$ the convergence of the equilibrium becomes very slow. This slowing-down can be explained by essential changes of the boundary surface shape during the free-boundary VMEC run in the case of a rather big beta (see figure 1(*b*)). Therefore, to follow the tendency in the effective ripple behaviour, a well converged equilibrium with $\langle\beta\rangle \approx 1.5\%$ is used instead of an equilibrium with $\langle\beta\rangle \approx 3\%$. As it follows from figure 1, for $\langle\beta\rangle \approx 1.5\%$ the confinement region expands and the final boundary differs significantly from the starting boundary. This change of the boundary shape leads to some increase in the effective ripple in the vicinity of the plasma boundary (see figure 2). In this vicinity, the $\epsilon_{\rm eff}^{3/2}$ parameter is approximately two times larger than for the fixed boundary equilibrium with $\langle\beta\rangle \approx 3\%$ and bootstrap current.

It should be noted that $\epsilon_{\rm eff}^{3/2}$ for a conventional stellarator with the same size is in the range of $(1\text{–}3) \times 10^{-2}$.

In the ideal case of quasi-axial symmetry the harmonics B_{mn} should be absent in the Boozer spectrum of B for non-zero n (m and n are the poloidal and toroidal harmonic numbers). The effective ripple should be zero in such a case. However, for CHS-qa some small harmonics with non-zero n are present in Boozer spectrum of B and this results in the finite value of the effective ripple. From [9], the following list of the most important harmonics of B can be obtained: harmonics (1,0), (2,0), which correspond to quasi-axial symmetry, and harmonics (0,1), (−1,1), (1,1), (1,2), (2,2), which violate the quasi-symmetry. The latter harmonics are of essentially smaller amplitudes in comparison with the quasi-symmetric ones. In section 4.3, distributions of B on magnetic surfaces are considered (see figures 6–8). Note that in magnetic coordinates the ripple from the discrete character of modular coils is not considered; however, this ripple is taken into account for real-space calculations in the next subsection.

4.2. Effective ripple in real-space coordinates

In the following, results obtained for the vacuum field produced by modular coils are presented. Curves with label 1 in figure 3 show Poincaré plots of the outermost magnetic surface for the final version of the modular coils obtained after additional optimization.

To assess the sensitivity of the effective ripple to magnetic field perturbations, the magnetic field produced by the optimized modular coils is modified with a small additional homogeneous vertical magnetic field $B_\perp = \pm 0.01 B_0$. This additional vertical field results in an inward or outward shift of magnetic surfaces for $B_\perp > 0$ or $B_\perp < 0$, respectively, accompanied by a pertinent increase or decrease of the confinement region. In addition, figure 3 shows Poincaré plots of the outermost magnetic surfaces obtained with the additional vertical field. These surfaces correspond to the following starting points of integration in the $\varphi = 0$ plane for $z = 0$: $R_{st} = 1.671$ ($B_\perp > 0$); $R_{st} = 1.699$ ($B_\perp = 0$); and $R_{st} = 1.735$ ($B_\perp < 0$). Smaller values of R_{st} result in small-scale island surfaces and in the appearance of regions with stochastic behaviour of the magnetic field lines. A further decrease of R_{st} results in magnetic field lines that leave the confinement region.

The corresponding results for $\epsilon_{eff}^{3/2}$ are shown in figure 4, curve 1 for the case without perturbation. These results are not worse than the corresponding results obtained earlier in [8] for the preceding CHS-qa version $2w39$. However, the aspect ratio for $2b32$ (3.2) is smaller than the one for $2w39$ (3.9). In addition, figure 4 shows the results for the perturbed magnetic field. Also in these cases, the radius is normalized with the mean radius a of the outermost magnetic surface of the unperturbed case. For $B_\perp > 0$ the values of $\epsilon_{eff}^{3/2}$ are somewhat larger than for $B_\perp = 0$, whereas for $B_\perp < 0$ the values in a limited region are somewhat smaller. This correlates with corresponding results in [9] where it is shown that the $1/\nu$ diffusion coefficient is reduced in the case of an outward shifted $2b32$ configuration. However, one should bear in mind that the confinement volume for the outward shifted configuration is also decreased.

The sharp increases of $\epsilon_{eff}^{3/2}$ in figure 4 result from island magnetic surfaces ($\iota = \frac{4}{11}$ for $B_\perp = 0$ and $B_\perp < 0$, $\iota = \frac{6}{17}$ and $\frac{10}{28}$ for $B_\perp > 0$). Curve 4 in figure 3 show the most

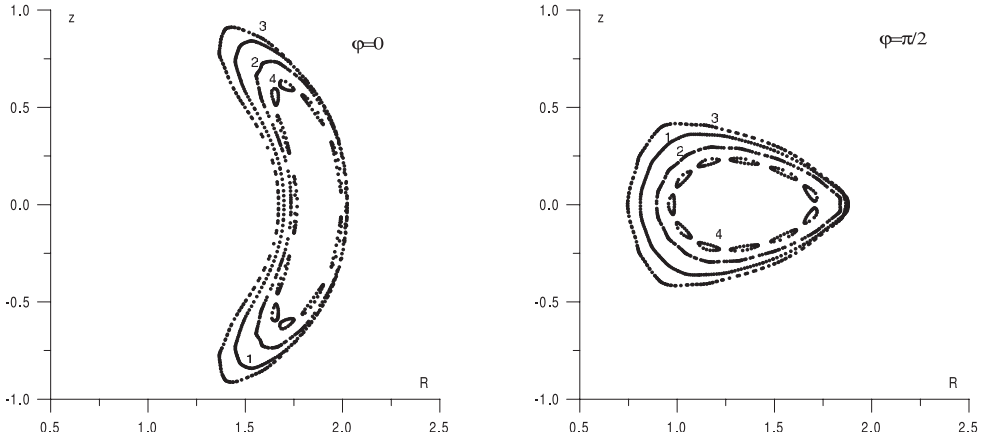

Figure 3. The outermost magnetic surfaces of the $2b32$ configuration for the vacuum magnetic field produced by modular coils for the unperturbed magnetic field and in the presence of an additional vertical homogeneous magnetic field $B_\perp$; 1: $B_\perp = 0$; 2: $B_\perp/B_0 = -0.01$ (outward shifted configuration); 3: $B_\perp/B_0 = 0.01$ (inward shifted configuration); 4: island surfaces $\iota = \frac{4}{11}$ for $B_\perp < 0$.

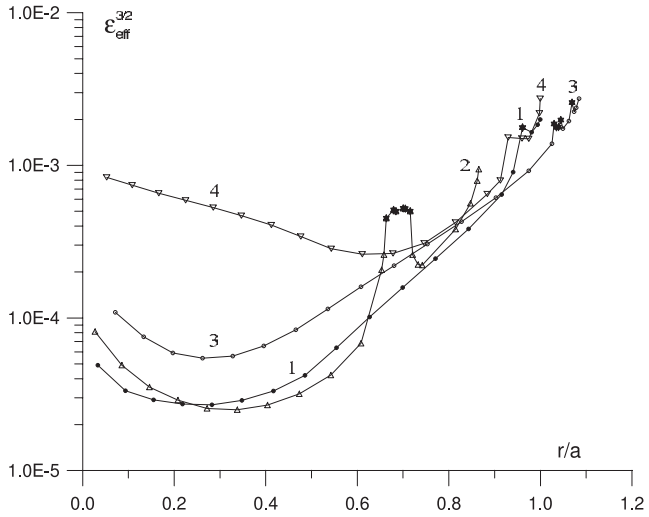

Figure 4. Parameter $\epsilon_{\rm eff}^{3/2}$ for the vacuum magnetic field of 2b32 in the presence of an additional vertical magnetic field $B_\perp$: for $B_\perp = 0$ (curve 1) and for $B_\perp/B_0 = \pm 0.01$ (curve 2 for the outward shifted configuration and curve 3 for the inward shifted configuration; a is the mean radius of the outermost surface for $B_\perp = 0$); thick markers show results for island surfaces. Curve 4 shows $\epsilon_{\rm eff}^{3/2}$ for the vacuum magnetic field produced by the modular coils 2b32s (before additional optimization).

evident island surfaces corresponding to the case of $B_\perp < 0$ for $\iota = \frac{4}{11}$. Different island surfaces are not presented in the figure since the corresponding islands are of smaller sizes and less visible in the figure scale. Inside the magnetic islands local magnetic configurations are formed with their own spatial axes. The increase of the effective ripple shows that for these local configurations the confinement properties can differ from those for the basic non-island magnetic surfaces.

Curve 4 in figure 4 shows the results corresponding to the modular coils of the 2b32s configuration. This is the initial modular coil system without any additional optimization to reduce the residual mirror ripple of the vacuum magnetic field. The only difference of configuration 2b32s from configuration 2b32 lies in somewhat different modular coil shapes (see [9]). In major parts of the confinement region, $\epsilon_{\rm eff}^{3/2}$ values for 2b32s are significantly larger than those for 2b32 although the values still do not exceed the corresponding values for W7-X.

4.3. Additional characteristics of the magnetic field

Some useful characteristics for the magnetic field of CHS-qa are presented in figures 5–8.

In figure 5, the rotational transform ι (in units of 2π) is presented for the Boozer version of 2b32 as well as for the field produced by modular coils. In all calculations, the θ coordinate is counted in clockwise direction and the sign '$-$' in ι means that the rotational transform has anti-clockwise direction with increasing φ. There is a very good coincidence of ι for the zero beta case in magnetic coordinates and for the vacuum field produced by modular coils.

For the finite beta case with zero toroidal current, the $|\iota|$ value slightly decreases in the direction to the centre of the configuration. In the finite beta cases with bootstrap current, a significant increase of $|\iota|$ is seen. From figure 5 one may expect that for finite beta cases during the discharge several low order islands can arise, which, however, cannot be analysed

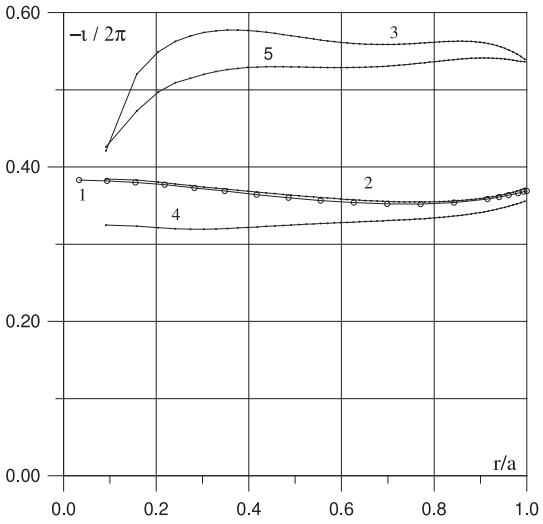

Figure 5. Rotational transform for the vacuum magnetic field produced by modular coils (curve 1) and for the magnetic field in Boozer coordinates: zero beta case (curve 2); fixed boundary equilibrium $\langle\beta\rangle \approx 3\%$ with bootstrap current (curve 3) and with negligible bootstrap current (curve 4); free boundary equilibrium $\langle\beta\rangle \approx 1.5\%$ with bootstrap current (curve 5).

in magnetic coordinates. As it follows from figure 4 for these islands the effective ripple can be increased.

Figures 6–8 show distributions of the normalized magnetic field strength ($b = B/B_0$) along magnetic field lines for the zero beta case in magnetic coordinates and for the field produced by modular coils. In figure 6, this quantity is shown for some inner magnetic surfaces including a surface for the vacuum field before any additional optimization of the modular coils ($2b32s$). For this surface, rather big magnetic field ripples $B_{0,1}$ are seen in contrast to the analogous magnetic surface for the vacuum field after additional optimization ($2b32$). This is in agreement with the corresponding results of [9] and explains the bigger effective ripple for the inner region of the vacuum field before the additional optimization of the modular coils. For the corresponding vacuum magnetic surface with an optimized modular coil system, the amplitude of the magnetic field ripples turns out to be essentially smaller. In this case, it is of the same order as for the magnetic field ripples in magnetic coordinates for the zero beta case. However, the number of local B minima for the field presented in magnetic coordinates is essentially smaller than that for the field produced by optimized modular coils. This is one of the reasons why $\epsilon_{\rm eff}^{3/2}$ computed for the field produced by the optimized modular coil system is larger than $\epsilon_{\rm eff}^{3/2}$ computed in magnetic coordinates for the zero beta case.

For some intermediate surface and for the outer magnetic surface the distribution of $b = B/B_0$ along the magnetic field line is shown in figures 7 and 8 for the zero beta case as well as for the vacuum field produced by the optimized modular coils, respectively. For equivalent magnetic surfaces with close ratios of r/a the characteristics of the curves for both magnetic field representations is rather close; however, in magnetic coordinates the curves are much smoother.

4.4. Bounce-averaged drift velocity across magnetic surfaces

The bounce-averaged drift velocity of the trapped particle is an important characteristic of the confinement properties of a stellarator configuration. The component of this velocity that

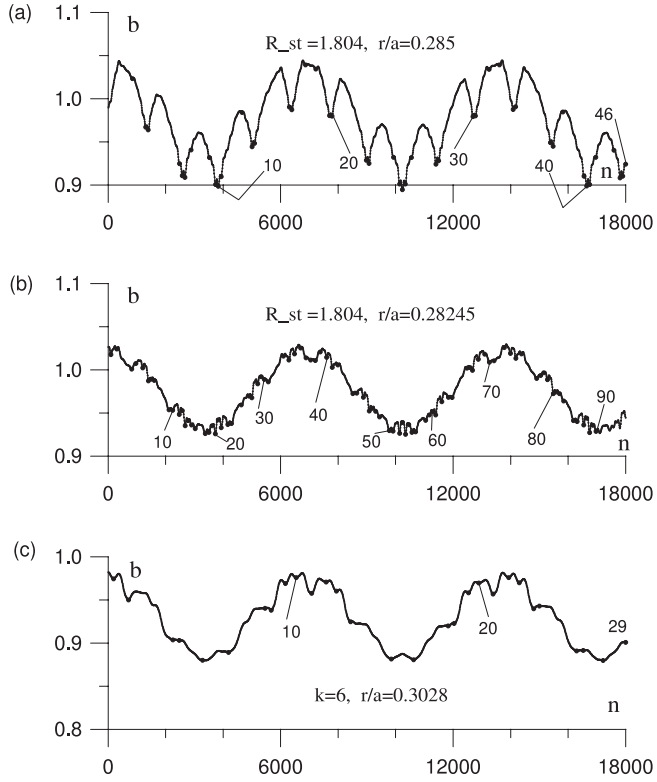

Figure 6. Distribution of $b = B/B_0$ along the magnetic field lines for the $2b32$ configuration for inner magnetic surfaces: for the vacuum magnetic field produced by modular coils for the $2b32s$ version (a), for the final version (b) and for the Boozer presentation of the magnetic field in the zero beta case (c); n is the number of integration steps with 1280 steps per magnetic field period; every 10th local minima of B is marked by the corresponding number.

is normal to the magnetic surface, $v_{\rm an}$, is of great interest since the asymmetric long-mean-free path transport is directly connected just with this quantity. In particular, an appropriate qualitative explanation of the effective ripple characteristics can be given with the help of this component. Here, the $v_{\rm an}$ quantity is studied for a number of magnetic surfaces of the $2b32$ configuration. The analogous study for CHS has already been carried out in [8]. Also for $v_{\rm an}$ computations, a method based on integration along magnetic field lines [11, 24] is used.

The $v_{\rm an}$ quantity is calculated for the local minima of B placed along a magnetic field line. The computational results are presented in a normalized form as a functional dependence between the dimensionless parameters η and γ with

$$\eta = \frac{R_0}{J_\perp B}\frac{\omega_{\rm c}}{\tau_{\rm b}}\frac{\delta\psi}{\langle|\nabla\psi|\rangle}, \qquad \gamma = \frac{v_{\parallel i}}{v_{\perp 0}}. \tag{6}$$

Here, $\tau_{\rm b}$ is the bounce time, $\delta\psi$ is the increment in ψ during $\tau_{\rm b}$, $v_{\perp 0} = \sqrt{J_\perp B_0}$, $\langle|\nabla\psi|\rangle$ is the averaged $|\nabla\psi|$ value for the magnetic surface under consideration, and $\omega_{\rm c} = eB/(mc)$ is the cyclotron frequency. The quantity $v_{\parallel i}$ is the parallel velocity $v_\parallel$ at the point of a local minimum of B for which the parameter η is calculated. The γ parameter is related to the pitch angle at the point of the local minimum of B or, accordingly, to the depth of particle trapping. In (6), the part $\delta\psi/(\tau_{\rm b}\langle|\nabla\psi|\rangle)$ directly represents $v_{\rm an}$ and the part $R_0\omega_{\rm c}/(J_\perp B)$ is of order of the inverse velocity of the ∇B drift. So, the parameter η is a normalized $v_{\rm an}$,

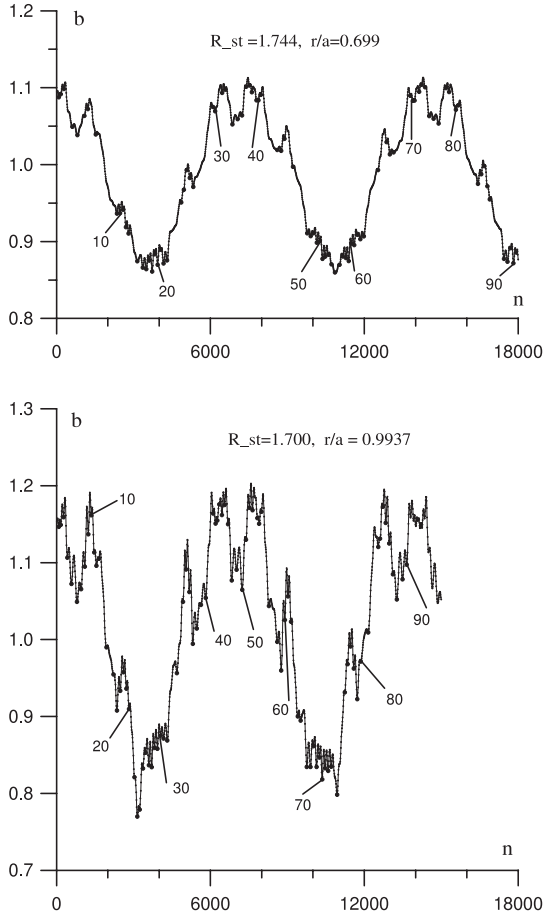

Figure 7. Same as figure 6 for intermediate and outer magnetic surfaces for the vacuum magnetic field produced by modular coils.

where the normalization is performed in such a way that for a conventional stellarator magnetic field [13], the result is $\eta = \eta_m \sin\vartheta$ where ϑ is the poloidal angle in quasi-toroidal coordinates and η_m=0.5.

Computations of η as functions of γ are done for minimum B points shown in figures 6–8. Some characteristic results of these computations are presented in figures 9 and 10. The curves are numbered in accordance with the numbering of the minima of B. The parameter η makes sense only for the γ interval $0 \leqslant \gamma \leqslant \gamma_{\max}$, which corresponds to the pitch angles of trapped particles. The $\gamma_{\max}$ value depends on the magnetic surface and the position of the corresponding minimum of B.

In figures 9 and 10, the results for the full γ interval, which corresponds to trapping within several minima of B, are shown only for a small number of curves. For such curves, transitions are seen between γ values corresponding to trapping within different numbers of ripple wells. They are marked by sharp changes of η. To avoid overloading of the figures, for most of the curves only the biggest η values are shown, which correspond to particles being trapped within one or two ripple wells.

Results of figure 9 relate to inner magnetic surfaces for the magnetic field produced by modular coils with and without additional optimization and to the zero beta case in magnetic

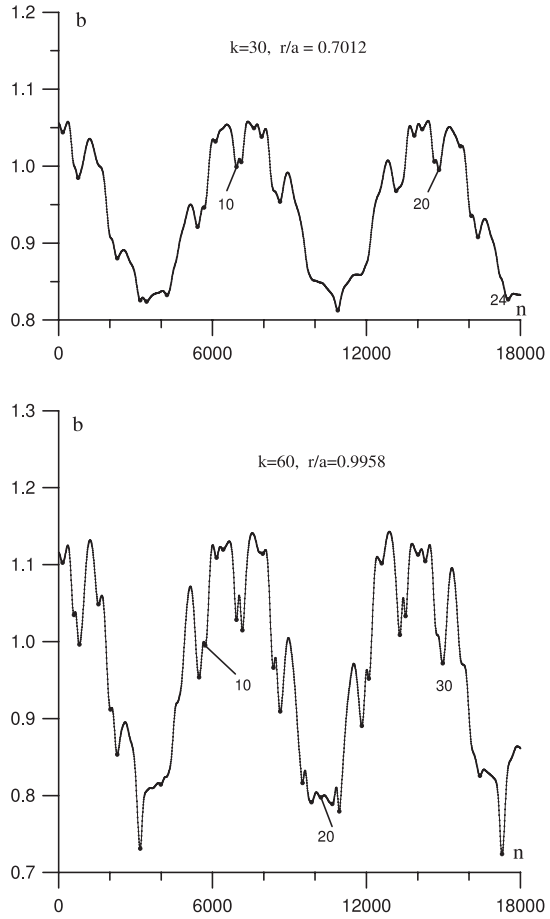

Figure 8. Same as figures 6 and 7 for the Boozer presentation of the magnetic field in the zero beta case (k shows the magnetic surface number).

coordinates. It can be seen that for all three cases the maximum values of η are about 0.25. However, the intervals of γ corresponding to the most important η values are larger for the vacuum field before additional optimization (0.2) than those for the vacuum field after additional optimization (0.1). The smallest values are obtained for the zero beta case in magnetic coordinates (0.05). This correlates well with the characteristics of $\epsilon_{\text{eff}}^{3/2}$ (see figures 2 and 4) obtained for these cases.

Figure 10 shows the results of η computations for intermediate magnetic surfaces of the vacuum magnetic field of the final version of modular coils and of the zero beta case in magnetic coordinates. It can be seen that for the vacuum field the maximum η values (0.3) are slightly larger than those for the zero beta case in magnetic coordinates (0.25). However, the intervals of γ corresponding to the most important η values are somewhat larger now for the zero beta case in magnetic coordinates. This compensates the role of the increase of η for the vacuum field and leads to the approximate coincidence of $\epsilon_{\text{eff}}^{3/2}$ for these two cases.

Results for the outer magnetic surfaces are not shown here. In general, it turns out that for the zero beta case in magnetic coordinates the maximum η reaches the value of 0.4 with corresponding γ intervals up to 0.2. In addition, for the field produced by optimized modular coils, a maximum η of 0.6 appears in rare cases with a corresponding γ of 0.1.

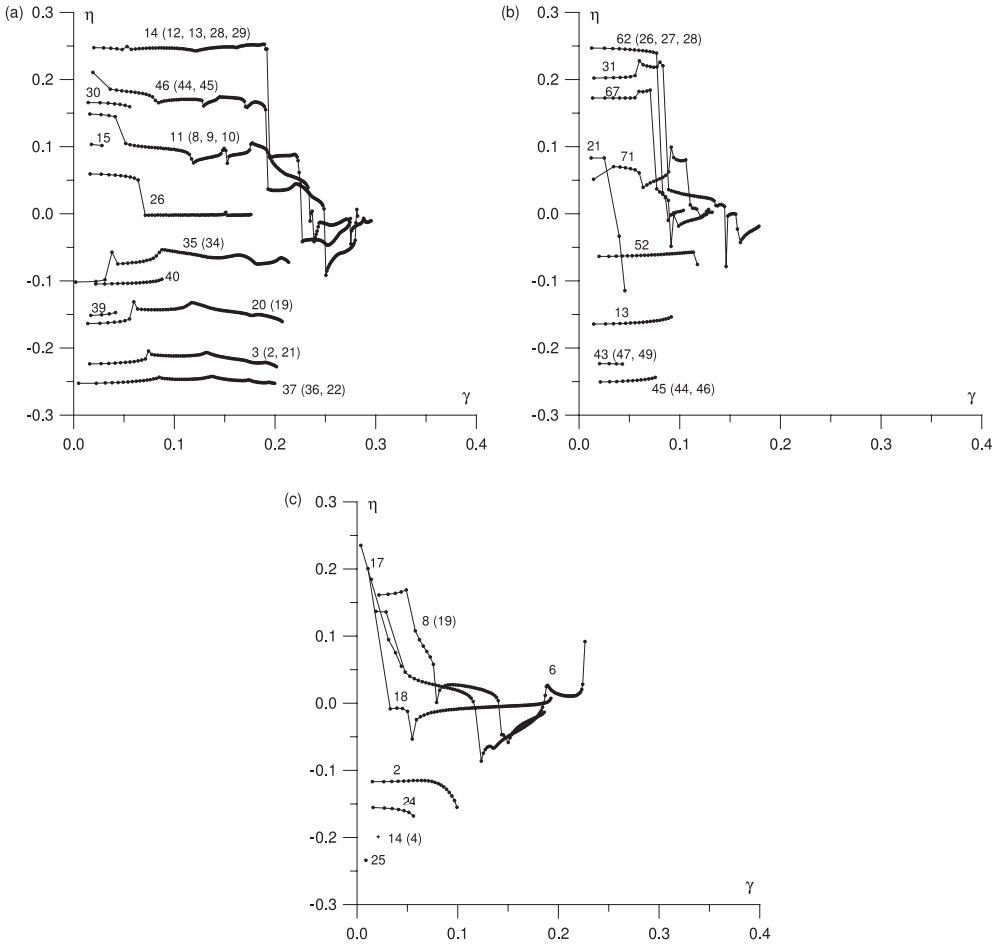

Figure 9. Parameter η as a function of γ for the $2b32$ configuration for inner magnetic surfaces. Curves are numbered according to the numbering of the minima of B along the field line (numbers of similar curves that are not shown are given in brackets): (*a*) $r/a = 0.285$, modular coils before additional optimization ($2b32s$); (*b*) $r/a = 0.282\,45$, modular coils (final version); (*c*) $r/a = 0.3028$, zero beta case in Boozer coordinates.

5. Comparison with CHS results

Here, a comparison of the main results with analogous results obtained for CHS in [8] is presented. In figure 11, $\epsilon_{\rm eff}^{3/2}$ is presented as function of r/a for two CHS configurations, the standard configuration and the drift-orbit-optimized (inward shifted) configuration. These results are compared to the favourable results of CHS-qa with and without bootstrap current. In particular, it has to be noted that the level of $\epsilon_{\rm eff}^{3/2}$ for $2b32$ is two orders of magnitude smaller than the one for the standard configuration of CHS.

6. Conclusions

A study of the effective ripple, $\epsilon_{\rm eff}$, in CHS-qa has been started in [8] where for the preceding CHS-qa version $2w39$ favourable results for $\epsilon_{\rm eff}$ were obtained. However, in [8] only the

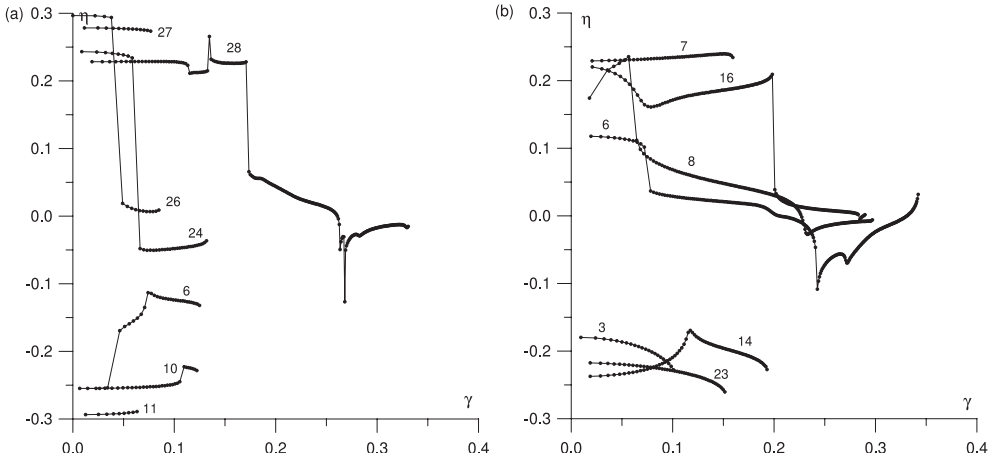

Figure 10. Same as figure 9 for intermediate magnetic surfaces: (*a*) $r/a = 0.699$, modular coils (final version); (*b*) $r/a = 0.7012$, zero beta case in Boozer coordinates.

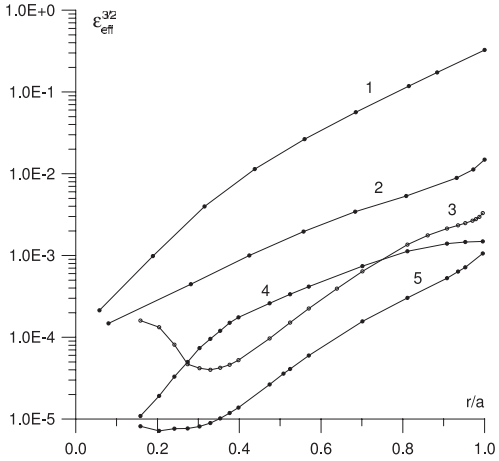

Figure 11. Parameter $\epsilon_{\rm eff}^{3/2}$ compared to results of CHS: CHS, standard configuration (curve 1); CHS, drift-orbit-optimized (inward shifted) configuration (curve 2); 2*b*32, free boundary equilibrium $\langle\beta\rangle \approx 1.5\%$ with bootstrap current (curve 3); 2*b*32, fixed boundary equilibrium $\langle\beta\rangle \approx 3\%$ with bootstrap current (curve 4); 2*b*32, zero beta (curve 5).

vacuum magnetic field produced by modular coils was considered. In this paper, the study of the effective ripple is continued for the new (final) version of CHS-qa (2*b*32) with a smaller aspect ratio. Now, in addition to vacuum magnetic fields produced by modular coils, finite beta equilibria in magnetic coordinates with and without bootstrap current are also studied.

The consideration starts from a zero beta case in magnetic coordinates and continues to the vacuum magnetic field produced by modular coils. The shape and the currents in these coils were found in accordance with the boundary surface for the zero beta case. Such an approach is reasonable from the viewpoint of the possibility of a low beta operation in the experiment. To find $\epsilon_{\rm eff}$ features that correspond to higher beta values and finite bootstrap current, the same boundary is used to obtain Boozer data for finite beta equilibria of $\langle\beta\rangle \approx 3\%$ with zero toroidal current as well as with finite bootstrap current.

For the zero beta case in magnetic coordinates and for the vacuum magnetic field produced by modular coils, $\epsilon_{\rm eff}^{3/2}$ stays below 10^{-4} for a significant part of confinement region (except the near-edge part). This is the same level as reported for the quasi-helically symmetric stellarator [23]. The representation as $\epsilon_{\rm eff}^{3/2}$ is convenient since the $1/\nu$ transport coefficients are directly proportional to this parameter. Near the edge, $\epsilon_{\rm eff}^{3/2}$ turns out to be not larger than 2×10^{-3}. An additional vertical magnetic field of $\pm 1\%$ of the toroidal field does not strongly increase (decrease) the effective ripple for the vacuum configuration. At the same time, this field leads to an increase (decrease) of the confinement region and to an inward (outward) shift of the configuration. It should be noted that near the edge of the configuration and for its inner part $\epsilon_{\rm eff}$ for the vacuum magnetic field produced by modular coils is somewhat larger than $\epsilon_{\rm eff}$ calculated in magnetic coordinates for the zero beta case. Relatively small additional magnetic field ripples corresponding to discrete coils explain this increase.

For the finite beta equilibrium with bootstrap current, $\epsilon_{\rm eff}^{3/2}$ is found to be larger than for the zero beta case. However, in general, the level of $\epsilon_{\rm eff}^{3/2}$ does not exceed the value of approximately 10^{-3} and is two orders of magnitude smaller than the level for the standard configuration of CHS.

The computational results for the bounce-averaged trapped particle drift velocity across magnetic surfaces and the corresponding pitch angles correlate well with the obtained $\epsilon_{\rm eff}$ values.

The $\epsilon_{\rm eff}^{3/2}$ level of 10^{-3} obtained for the fixed boundary equilibrium corresponds to the $\epsilon_{\rm eff}$ value of 10^{-2}. An effective ripple of this order (1.5%) is reported in [10] for W7-X. So, for the fixed boundary equilibrium the effective ripple for CHS-qa does not exceed the corresponding level in W7-X.

For the free boundary VMEC equilibrium it turned out that with increasing beta the convergence of the equilibrium with a finite bootstrap current becomes very slow. Therefore, to follow the tendency in the effective ripple behaviour, instead of an equilibrium for $\langle\beta\rangle \approx 3\%$, a well converged equilibrium for $\langle\beta\rangle \approx 1.5\%$ is considered. For this beta value, the confinement region expands and the boundary shape undergoes some changes. This leads to some increase in the effective ripple in the vicinity of the plasma edge. However, for $\langle\beta\rangle \approx 1.5\%$ this increase is not dramatic ($\epsilon_{\rm eff}^{3/2} = 3.3 \times 10^{-3}$) and the effective ripple for CHS-qa remains essentially smaller than that for the conventional stellarator.

In comparing various stellarator devices one should bear in mind that $\epsilon_{\rm eff}^{3/2}$ is normalized with R_0^2. Therefore, with identical values for the effective ripple, particle and energy fluxes in the $1/\nu$ regime scale with $1/R_0^2$, thus making transport smaller in larger devices.

Acknowledgments

This work was partly supported by the 'Monbusho International Scientific Research Program: Joint Research' (Japan), by the Austrian Academy of Sciences and by the Association EURATOM-OEAW. The contents of the publication is the sole responsibility of its publishers and it does not necessarily represent the views of the Commission or its services. The authors would like to thank Prof. N Nakajima for help with the free boundary VMEC equilibrium.

References

[1] Matsuoka K, Okamura S, Fujiwara M, Drevlak M, Merkel P and Nührenberg J 1997 *Plasma Phys. Rep.* **23** 542–6

[2] Okamura S, Matsuoka K, Fujiwara M, Drevlak M, Merkel P and Nührenberg J 1998 *J. Plasma Fusion Res. Ser.* **1** 164–7

[3] Okamura S *et al* 2000 *27th EPS Conf. on Controlled Fusion and Plasma Physics (Budapest, Hungary, 12–16 June 2000)* ed K Szego *et al Report* P4.018
[4] Matsuoka K *et al* 1989 *Proc. 12th Int. Conf. on Plasma Physics and Controlled Nuclear Fusion Research 1988 (Nice, 1988)* vol 2 (Vienna: IAEA) pp 411–17
[5] Okamura S *et al* 1999 *Nucl. Fusion* **39** 1337
[6] Okamura S *et al* 2001 *Nucl. Fusion* **41** 1865–71
[7] Shimizu A, Okamura S, Isobe M, Suzuki C, Nishimura S, Nomura I and Matsuoka K 2001 *J. Plasma Fusion Res. Ser.* **4** 461–5
[8] Heyn M F, Isobe M, Kasilov S V, Kernbichler W, Matsuoka K, Nemov V V, Okamura S and Pavlichenko O S 2001 *Plasma Phys. Control. Fusion* **43** 1311–24
[9] Shimizu A, Okamura S, Isobe M, Suzuki C, Nishimura S, Watari T and Matsuoka K 2003 *Fusion Eng. Des.* **65** 109–18
[10] Grieger G *et al* 1992 *Phys. Fluids* B **4** 2081
[11] Nemov V V, Kasilov S V, Kernbichler W and Heyn M F 1999 *Phys. Plasmas* **6** 4622
[12] Boozer A A 1981 *Phys. Fluids* **24** 1999
[13] Galeev A A and Sagdeev R Z 1979 *Reviews of Plasma Physics* vol 7, ed M A Leontovich (New York: Consultants Bureau) p 257 (see also in 1973 *Voprosy Teorii Plazmy* vol 7 (Moscow: Atomizdat) p 205 (in Russian))
[14] Nemov V V 1988 *Nucl. Fusion* **28** 1727
[15] Nemov V V, Kasilov S V, Kernbichler W and Heyn M F 2001 Evaluation of an effective ripple in stellarators *28th EPS Conf. on Controlled Fusion and Plasma Physics (Madeira, Portugal, 18–22 June 2001) Report* P5.055
[16] Hirshman S P, Van Rij W I and Merkel P 1986 *Comput. Phys. Commun.* **43** 143
[17] Watanabe K Y, Nakajima N, Okamoto M, Yamazaki K, Nakamura Y and Wakatani M 1995 *Nucl. Fusion* **35** 335
[18] Isobe M *et al* 2001 Neoclassical bootstrap current in CHS-qa quasi-axisymmetric stellarator *28th EPS Conf. on Controlled Fusion and Plasma Physics (Madeira, Portugal, 18–22 June 2001) Report* P2.075
[19] Isobe M, Okamura S, Nakajima N, Shimizu A, Nishimura S, Suzuki C, Murakami S, Fujisava A and Matsuoka K 2002 *J. Plasma Fusion Res. Ser.* **5** 360–5
[20] Merkel P 1987 *Nucl. Fusion* **27** 867
[21] Drevlak M 1998 *Fusion Technol.* **33** 106
[22] Nemov V V, Kasilov S V, Nührenberg C, Nührenberg J, Kernbichler W and Heyn M F 2003 *Plasma Phys. Control. Fusion* **45** 43
[23] Nührenberg J and Zille R 1988 *Phys. Lett.* A **129** 113
[24] Nemov V V 1999 *Phys. Plasmas* **6** 122